Eur. Phys. J. D **17**, 205–212 (2001)

THE EUROPEAN PHYSICAL JOURNAL D

EDP Sciences
© Società Italiana di Fisica
Springer-Verlag 2001

Structural and vibrational properties of C_{36} and its oligomers $(C_{36})_{M=2,3,4}$ by tight-binding molecular dynamics

T.A. Beu[1,a], J. Onoe[2], and K. Takeuchi[2]

[1] University "Babeş-Bolyai", Faculty of Physics, 3400 Cluj-Napoca, Romania
[2] The Institute of Physical and Chemical Research (RIKEN), Wako-shi, 351-01 Saitama, Japan

Received 24 November 2000 and Received in final form 24 August 2001

Abstract. Non-orthogonal tight-binding molecular-dynamics is employed to calculate structural and vibrational properties of C_{36} and its oligomers $(C_{36})_{M=2,3,4}$. The lowest energy configuration of the C_{36} cage is confirmed to have D_{6h} symmetry. For the dimer, too, the D_{2h} structure reported in the literature is found. The vibrational spectrum is identified with the power spectrum of the displacement autocorrelation function. Additional vibrational properties are extracted from the dynamical matrix. For the monomer, fair agreement with available *ab initio* calculations is achieved, with comparatively smaller deviations in the Raman-frequencies than for published semi-empirical calculations. The features of the vibrational modes are correlated with the structural properties of the oligomers.

PACS. 31.15.Qg Molecular dynamics and other numerical methods – 71.20.Tx Fullerenes and related materials; intercalation compounds – 33.20.Ea Infrared spectra

1 Introduction

Various properties of C_{36} molecules have been investigated experimentally over the last several years [1–4]. However, the synthesis of solid form C_{36} was achieved only recently [5]. Solid-state NMR measurements indicate that the molecule has D_{6h} symmetry and the electron diffraction patterns suggest the crystal has hexagonal symmetry. The IR absorption spectrum of the powdered crystal shows a number of broad features between 400 and 1 800 cm^{-1} and, to our knowledge, no other measurements of vibrational frequencies of C_{36} have been reported.

The electronic and structural properties of several isomers of molecular C_{36} were recently investigated by Grossman *et al.* [6] and Côté *et al.* [7]. Full structural relaxations and electronic density of states were evaluated using an *ab initio* pseudopotential density functional (DFT) approach. Two carbon cages with 8 hexagons and 12 pentagons, one with D_{6h} symmetry (in agreement with the experimental findings), and the other with D_{2d} symmetry, were found to be the most stable, with bond lengths of the order of those in C_{60} and C_{70}.

The most elaborate calculations of the vibrational frequencies of C_{36} reported up to now are the first-principles calculations of Jishi *et al.* [8], using a spin-polarized DFT approach within the local density approximation (LDA). For the IR spectrum, the overall agreement of the calculated frequencies with the experimental data is very good. Calculated frequencies for the Raman-active modes are reported as well.

Using a semi-empirical covalent potential which was shown to work well for C_{60} and C_{70}, Halac *et al.* [9] explored possible geometrical structures and calculated the IR and the Raman spectrum of C_{36}. In agreement with the *ab initio* calculations, the D_{6h} and D_{2d} structures were found again to be the most stable. Fowler *et al.* [10] reported structures and energies, calculated at the density-functional tight-binding (DFTB) level, for C_{36}-based fullerenes, oligomers, and solids. It is found that C_{36} forms stronger inter-cage bonds than larger fullerenes.

Our interest in C_{36} is driven by the persistent incomplete experimental evidence (mainly concerning the Raman spectrum), as well as by the speculations of Fowler *et al.* about the potential role of C_{36} as building block in fullerene compounds and solids. Since local density approximation (LDA) calculations for fullerene oligomers (involving full geometry optimization and subsequent structural and vibrational analysis) are indeed out of reach of many powerful computers, there is a clear need for alternative approaches, implying less computational effort and preserving, at the same time, the level of accuracy of LDA methods. Tight-binding (TB) schemes, extensively applied in the last two decades to investigate covalent systems, have proved to be valuable candidates. They can be viewed as simplified two-center-oriented *ab initio* methods, since the electronic properties of the system are calculated quantum mechanically.

[a] e-mail: tbeu@phys.ubbcluj.ro

The TB parametrization employed in the present study is the elaborate and yet conveniently implementable scheme proposed by Papaconstantopoulos *et al.* [11–13], which we recently have shown to very accurately describe the structure and experimental Raman spectrum of C_{60} [14]. As clearly follows from the obtained results, this high quality parametrization makes our TBMD approach comparable to *ab initio* methods in accuracy and definitely more economical, thus making large scale calculations possible at reasonable computational costs.

Section 2 contains a brief outline of the non-orthogonal TBMD formalism employed and of the TB parametrization considered. In Section 3 the obtained geometrical structures and considerations on the involved energetics are presented. Section 4 is devoted to the description of the methodology used and of the vibrational properties calculated.

2 Non-orthogonal tight-binding MD

In tight-binding total-energy (TBTE) models based on the Kohn-Sham *ansatz* to density-functional theory [15], the total energy of the system can be expressed as the sum of the "band structure energy" (sum of occupied one-electron energies) and a short-range repulsive pair potential (accounting for the corrections to the single-particle picture):

$$E_{\rm tot}(\{\mathbf{R}_J\}) = \sum_{k=1}^{n_{\rm occ}} n_k \varepsilon_k(\{\mathbf{R}_J\}) + \sum_{J<K} V_{\rm rep}(|\mathbf{R}_J - \mathbf{R}_K|). \tag{1}$$

The one-electron energies ε_k are eigenvalues of the characteristic equation:

$$(\mathbf{H} - \varepsilon_k \mathbf{S})\mathbf{C}^k = 0, \tag{2}$$

where the Hamiltonian matrix, $\mathbf{H}$, and the overlap matrix, $\mathbf{S}$, are expressed relative to some non-orthogonal set of atom-centered orbitals. $\mathbf{C}^k$ is the eigenvector corresponding to eigenvalue ε_k.

Most TBTE models use a parametrized pair potential to represent the repulsive contribution to the total energy. However, the Kohn-Sham formulation allows the eigenvalues to be shifted by an arbitrary constant. The TB parametrization of Papaconstantopoulos *et al.* [13], used throughout in this work, eliminates the pair potential by choosing the arbitrary zero for each band structure such that the total energy is given solely by the sum of the (shifted) one-electron energies.

The forces acting on the atoms are related to the gradients of the total energy at the atom sites and, according to equations (1) (without repulsive term) and (2), they are formally:

$$\mathbf{F}_I = -\frac{\partial E_{\rm tot}}{\partial \mathbf{R}_I} = -\sum_{k=1}^{n_{\rm occ}} \frac{n_k}{\mathbf{C}^{k\dagger}\mathbf{S}\mathbf{C}^k} \mathbf{C}^{k\dagger} \left(\frac{\partial \mathbf{H}}{\partial \mathbf{R}_I} - \varepsilon_k \frac{\partial \mathbf{S}}{\partial \mathbf{R}_I} \right) \mathbf{C}^k.$$

Within the parametrization considered they can be expressed analytically, this being an essential advantage with a view to tractable large-scale MD simulations.

Within a conventional orthogonal TB formalism, the bond orbitals for the tetrahedral structure are constructed from sp^3 hybrids. The use of sp^3 bonding for fullerenes is justified by the fact that the nominal sp^2 bonding between adjacent carbon atoms actually occurs on a curved surface, which leads to some admixture of sp^3 bonding. The total number of electrons considered for a molecule composed of N atoms is $n = 4N$. The corresponding number of occupied one-electron states is $n_{\rm occ} = n/2$, while the occupation number is $n_k = 2$. The $(4N) \times (4N)$ Hamiltonian matrix for the system of the valence electrons is consequently composed of 4×4 blocks corresponding to the coupling between the s, p_x, p_y and p_z orbitals of the involved atoms:

$$\mathbf{H} = \begin{bmatrix} \ddots & \vdots & & & \vdots & \vdots & & & \vdots & \\ \cdots & h_s^I & 0 & 0 & 0 \cdots & H_{ss}^{IJ} & H_{sx}^{IJ} & H_{sy}^{IJ} & H_{sz}^{IJ} & \cdots \\ & 0 & h_p^I & 0 & 0 & -H_{sx}^{IJ} & H_{xx}^{IJ} & H_{xy}^{IJ} & H_{xz}^{IJ} & \\ & 0 & 0 & h_p^I & 0 & -H_{sy}^{IJ} & H_{xy}^{IJ} & H_{yy}^{IJ} & H_{yz}^{IJ} & \\ \cdots & 0 & 0 & 0 & h_p^I \cdots & -H_{sz}^{IJ} & H_{xz}^{IJ} & H_{yz}^{IJ} & H_{zz}^{IJ} & \cdots \\ & \vdots & & & \vdots \ddots & \vdots & & & \vdots & \end{bmatrix}.$$

The diagonal *on-site* elements h_l^I ($l = s$ or p) can be assigned the simplified interpretation of atomic energies, but should generally be allowed to vary according to the local environment of each atom. For the Hamiltonian matrix elements of the non-diagonal block (I, J) the Slater-Koster form is usually considered [16]. In terms of bond direction cosines (γ_x^{IJ}, γ_x^{IJ} and γ_x^{IJ}) and two-center *hopping parameters* ($H_{ss\sigma}$, $H_{sp\sigma}$, $H_{pp\sigma}$, $H_{pp\pi}$), the relevant elements are expressed as:

$$\begin{cases} H_{ss}^{IJ} = H_{ss\sigma}^{IJ}, \\ H_{sx}^{IJ} = \gamma_x^{IJ} H_{sp\sigma}^{IJ}, \\ H_{xy}^{IJ} = \gamma_x^{IJ}\gamma_y^{IJ}\left(H_{pp\sigma}^{IJ} - H_{pp\pi}^{IJ}\right) + H_{pp\sigma}\delta_{xy}, \end{cases} \tag{3}$$

the remaining ones resulting from a straightforward permutations of indices x, y and z. Here $\delta_{\alpha\beta}$ is the Kronecker symbol.

In a *non-orthogonal* TB formulation, except for the unitary diagonal, the block-structure of the overlap matrix $\mathbf{S}$ is similar to the one of the Hamiltonian.

The TB parametrization of Papaconstantopoulos *et al.* [13] describes the environment of each atom by a pseudo-atomic density:

$$\rho_I = \sum_{J \neq I}^{N} \exp\left(-\lambda^2 R_{IJ}\right) f(R_{IJ}).$$

This depends exponentially on the distances to all neighbors and also through the cutoff function:

$$f(R) = \frac{1}{1 + \exp[(R - R_{\rm c})/\Delta]}.$$

The latter practically vanishes when $R > R_{\rm c}$, the main decrease taking place roughly within a domain of size Δ. For carbon the values $R_{\rm c} = 10.5\ a_0$ and $\Delta = 0.5\ a_0$ are employed (a_0 is the Bohr radius).

Table 1. Comparison of calculated bond lengths (in Å) for the D_{6h}-symmetry isomer of C_{36}.

Bond	Grossman[a]	Jishi[b]	Halac[c]	this work
d_1 (top and bottom hexagons)	1.41	1.43	1.46	1.434
d_2 (between adjacent pentagons)	1.48	1.42	1.49	1.440, 1.502
d_3 (between pentagons and median hexagons)	1.43	1.47	1.47	1.438, 1.427
d_4 (across the median hexagon belt)	1.43	1.40	1.43	1.428

[a] Reference [6] (pseudopotential DFT approach).
[b] Reference [8] (spin-polarized DFT LDA calculation).
[c] Reference [9] (semi-empirical calculation).

The (diagonal) on-site Hamiltonian elements are given in terms of the local pseudo-atomic density by a Birch-like equation:

$$h_l^I = \alpha_l + \beta_l \rho_I^{2/3} + \gamma_l \rho_I^{4/3} + \chi_l \rho_I^2,$$

where, obviously, only $l = s, p$ are considered. As for the two-center Slater-Koster hopping terms, they have been parametrized as polynomials times an exponential cutoff in order to exhibit the proper behavior for small interatomic distances ($\mu = \sigma, \pi$):

$$H_{ll'\mu}(R) = (a_{ll'\mu} + b_{ll'\mu} R + c_{ll'\mu} R^2) \exp\left(-d_{ll'\mu}^2 R\right) f(R)$$
$$S_{ll'\mu}(R) = (\delta_{ll'} + p_{ll'\mu} R + q_{ll'\mu} R^2 + r_{ll'\mu} R^3) \times \exp\left(-s_{ll'\mu}^2 R\right) f(R).$$

These then provide in virtue of relations (3) the non-diagonal Hamiltonian and overlap matrix elements for the overall system.

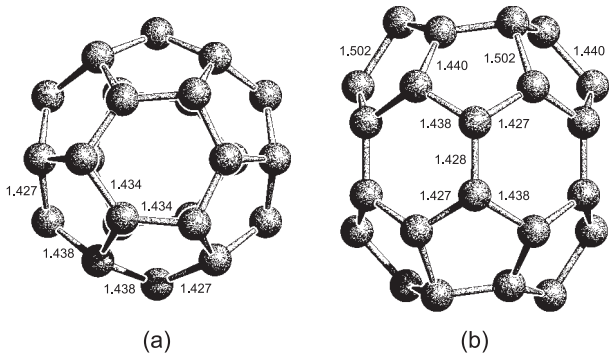

Fig. 1. Calculated structure of the D_{6h}-symmetry isomer of C_{36}: (a) top view, (b) side view. The relevant bond lengths are indicated in Å.

3 Structure and energetics

The equilibrium geometry of the C_{36} carbon cage was obtained by simulated annealing. The initial configuration was prepared by a random distortion of the regular D_{6h} configuration employed by Jishi *et al.* [8], which features 8 hexagonal and 12 pentagonal faces and is characterizable by four bond lengths. The distorted structure was allowed to relax for 1 ps with a time step of 2×10^{-4} ps, by reducing the velocities by 1% after each time step. The obtained relaxed structure is depicted in Figures 1a and 1b, top and side view, respectively.

As can be easily noticed, even though the carbon cage preserves the D_{6h} symmetry reported in the literature, it is no longer composed of regular pentagons and hexagons, but rather slightly distorted. Basically, the atoms of the top and bottom hexagons no longer lie in the same plane, but occupy slightly displaced, alternating positions above and beneath the respective plane. Thus the neighboring distorted pentagons are grouped in three symmetric pairs, forming the lower and the upper belt. The structure can be characterized by six (no longer four) bond lengths (see Tab. 1), even though these are changed quite little as compared to those of Jishi *et al.* (by less than 0.08 Å). On the whole, the distance between the corresponding atoms of the top and bottom hexagons is increased to 5.18 Å, making our structure slightly more elongated (by approximately 0.3 Å). As a matter of fact, a small geometric distortion (≤ 0.01 Å in D_{6h}-equivalent bonds) of the C_{36} cage has been also predicted by Fowler *et al.* [10].

It is interesting that our bond lengths seem to agree somewhat better with those resulted from the pseudopotential DFT calculations of Grossman *et al.* [6]. The maximum difference in this case amounts to 0.04 Å and corresponds to the three shorter bonds across the pentagon belts.

Though of the same order, as can be seen from Table 1, the bond lengths yielded by the semi-empirical calculations of Halac *et al.* depart more than ours from the *ab initio* results of references [6,8].

The equilibrium geometries of the oligomers were determined by simulated annealing, as well. For each oligomer several full geometry optimizations were performed, each starting from relative monomer positions favored by the symmetry of the relaxed C_{36} cage. The lowest energy configurations found for the oligomers are depicted in Figure 2 and they show well-defined symmetry: D_{2h} for the dimer, D_{3h} for the trimer, and D_{4h} for the tetramer. While the dimer and trimer form double bonds between the monomers (by face-to-face polar-polar connection of hexagons from the median belt of each involved cage), the tetramer binds the monomers by four-fold bonds (two pairs of equal bonds). Moreover, in the tetramer the C_{36} cages appear most deformed due to the less adapted symmetry of the environment.

Further relevant structural and energetic data are gathered in Table 2. As can be seen, due to the different

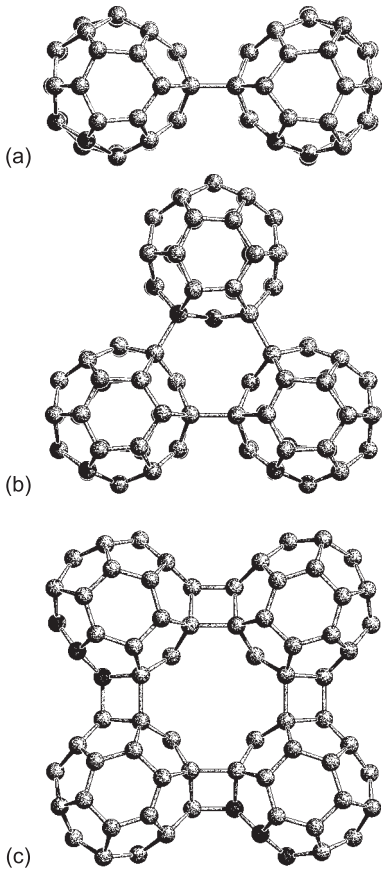

Fig. 2. The energetically most stable oligomers $(C_{36})_{M=2,3,4}$.

Table 2. Calculated inter-cage bond length, l, center-to-center inter-cage distance, d (both in Å), binding energy per atom, E_B, and band gap, Δ (both in eV).

	symmetry	l	d	E_B	Δ
C_{36}		-	-	9.74	0.37
$(C_{36})_2$	D_{2h}	1.60	6.69	9.77	1.26
$(C_{36})_3$	D_h	1.65	6.63	9.77	1.00
$(C_{36})_4$	D_{4h}	1.51 1.66	6.50	9.76	0.99

deformations of the contained monomers, the inter-cage bond length, l, is increased roughly by 0.05 Å in the trimer and tetramer as compared to the dimer. Nevertheless, the shorter (outer) inter-cage bonds of the tetramer measure only 1.51 Å. Quite on the contrary, the dimer shows the largest center-to-center inter-cage distance, $d = 6.69$ Å, the trimer and tetramer being thus slightly more compact on the whole.

It should be noted that for the dimer the geometrical data are in excellent agreement with those obtained by Fowler *et al.* from DFTB calculations ($l = 1.60$ Å and $d = 6.74$ Å).

The calculated binding energies per atom, E_B, are probably somewhat overestimated, since the used TB parametrization of Papaconstantopoulos *et al.* [13] is based on fits to LDA results for solids, and LDA is notorious for overbinding solids. Both in the dimer and trimer

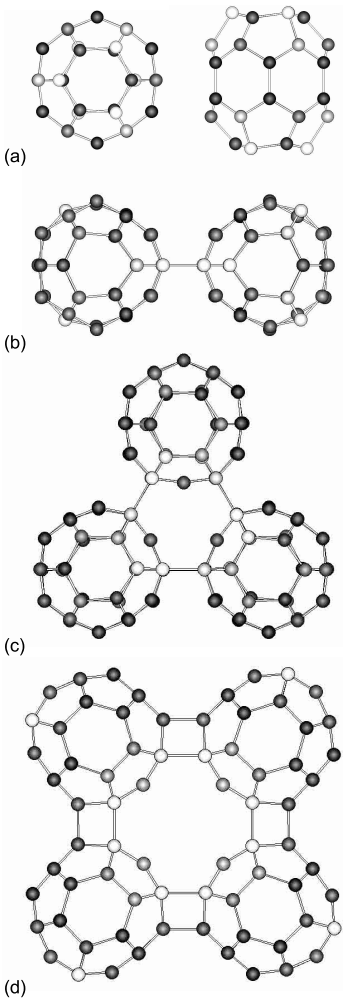

Fig. 3. Pseudo-atomic densities for the C_{36} fullerene and its oligomers $(C_{36})_{M=2,3,4}$.

(with 9.77 eV/atom) the atoms appear to be stabilized by an excess of 0.03 eV as compared to the monomer. Even though geometrically more compact, the tetramer (with 9.76 eV/atom) turns out to be slightly weaker bound. This can also be related to the more pronounced symmetry loss of the C_{36} cages within the tetramer.

The C_{36} molecule has a quite modest HOMO-LUMO gap, $\Delta = 0.37$ eV. All three considered oligomers have significantly higher HOMO-LUMO gaps, and this finding agrees again with the calculations of Fowler *et al.* [10].

In Figure 3 we have displayed by grey-levels the pseudo-atomic density for the C_{36} molecule and its considered oligomers. A darker shade corresponds to a higher value of the pseudo-density, thus implying a higher population. In the case of the monomer (Fig. 3a, top and side view), the highest-density sites are located (1) at the common vertices of the hexagons composing the median belt and (2) at the vertices of the top and bottom hexagons (alternating with low-density sites). Both for the dimer and trimer, the bonding atoms are low-density sites, higher densities occurring *around* the inter-cage bonds. This behavior is similar to the one reported by Esfarjani *et al.* [17]

for the charge distribution in the dumbbell isomer of the C_{60} dimer.

In the case of the tetramer, the inner (longer) inter-cage bonds are formed between low-density sites, while the outer (shorter) inter-cage bonds involve high-density sites. Roughly speaking, the high-density sites are preferentially located in the exterior "saddles" formed between the component monomers.

4 Vibrational properties

In order to characterize the overall vibration of the carbon cage, we employed the *displacement autocorrelation function*:

$$C_{\delta\mathbf{r}}(t) = \frac{\sum_{I=1}^{N}\langle\delta\mathbf{r}_I(t)\cdot\delta\mathbf{r}_I(0)\rangle}{\sum_{I=1}^{N}(\delta\mathbf{r}_I(0))^2},$$

with $\delta\mathbf{r}_I(t)$ representing the displacement of atom I at time t. The Fourier-transform (power spectrum) of $C_{\delta\mathbf{r}}(t)$ can be straightforwardly identified with the vibrational spectrum of the molecule. We did not use the more popular velocity autocorrelation function, since the initial preparation of the vibrational state and, consequently, also its subsequent monitoring can be more conveniently accomplished in terms of atomic displacements. Aside from this aspect, the information contained in the two autocorrelation functions is absolutely equivalent.

The vibration of molecules with an inversion point (such as C_{36}) can be additionally characterized by the *parity*, which we define as:

$$P = \frac{\sum_{I=1}^{N}\langle\delta\mathbf{r}_I\cdot(-\delta\mathbf{r}_{\mathrm{sym}(I)})\rangle}{\sum_{I=1}^{N}(\delta\mathbf{r}_I)^2},$$

where $\mathrm{sym}(I)$ designates the symmetric atom for atom I with respect to the inversion point.

An alternative way to analyze the vibrational properties within the harmonic approximation, providing also complementary information to those extracted from the power spectrum of autocorrelation functions, is based on the dynamical matrix [18].

For this approach to be applicable, one has to start from a fully relaxed geometrical structure of the molecular aggregate under consideration, with each atom occupying an equilibrium position. The elements of the dynamical matrix have the significance of local curvatures of the potential energy surface at the atom sites, and they can be approximated in the second order by the finite difference formula:

$$\mathcal{H}_{IJ}^{\alpha\beta} = -\frac{F_I^{\alpha}(r_J^{\beta}+h) - F_I^{\alpha}(r_J^{\beta}-h)}{2h} + O(h^2),$$
$$I,J = 1,2,\ldots,N, \quad \alpha,\beta = x,y,z,$$

with $F_I^{\alpha}(r_J^{\beta}\pm h)$ representing the α-component of the force acting on atom I when atom J is displaced by $\pm h$ along direction β.

In order to obtain the vibrational frequencies and the corresponding atomic displacements for the normal modes, one has to solve then the generalized eigenvalue problem for the dynamical matrix:

$$\mathcal{H}\cdot\delta\mathbf{r}_k = \omega_k^2\mathbf{M}\cdot\delta\mathbf{r}_k, \quad k = 1,2,\ldots,3N.$$

Here ω_k is the eigenvalue (frequency) of normal mode k, $\delta\mathbf{r}_k$ is the corresponding eigenvector (having as components the atomic displacements), and $\mathbf{M}$ is the diagonal matrix with the atomic masses on the main diagonal.

We will start by describing the results obtained for the C_{36} monomer. The 102 vibrational modes of the D_{6h}-symmetry isomer of C_{36} can be grouped as follows:

$$\Gamma_{\mathrm{vib}} = \begin{cases} 6A_{1g} + 8E_{1g} + 9E_{2g} & \text{Raman-active} \\ 2A_{2g} + 5B_{1g} + 4B_{2g} & \text{silent} \\ 5A_{2u} + 8E_{1u} & \text{IR-active} \\ 3A_{1u} + 4B_{1u} + 5B_{2u} + 9E_{2u} & \text{silent.} \end{cases}$$

Since, the Raman-active modes have *gerade* symmetry, while the IR-active ones are *ungerade*, monitoring the parity of the vibration during an MD simulation allows for the nature of the resulted power spectrum to be identified.

Each MD run was started from the relaxed D_{6h} structure obtained as described above. The equilibrium configuration was initially prepared (excited) by displacements of the atoms according to patterns which will be explicitly detailed in what follows. All runs spanned a time interval of 2 ps and, to ensure the stability and accuracy of the propagation process, a time step of 2×10^{-4} ps was used.

For a random initial excitation of the carbon cage, the normalized parity of the vibration was found to be predominantly positive, typically exceeding 0.9 on the average, which implies that the composite vibration of the molecule had overwhelmingly *gerade* symmetry. This behavior is actually a direct result of the *uniform* character of the applied random excitation.

To restrict the calculation exciting only Raman-active modes, the initial displacements of the atoms, though random, must additionally have *gerade* symmetry. This can be simply achieved by picking up atoms randomly and assigning them random displacements, while assigning *inverted* displacements to the symmetric ones. Provided the propagation errors are kept under control, for such "random *gerade*" initial excitations the unitary parity of the vibration is conserved throughout the run. This has the important consequence that the power spectrum of the autocorrelation function can be directly related to the Raman-spectrum.

Since by its specific nature this approach does not deal with individual vibrational modes separately, in order to assign the obtained peaks, besides the random *gerade* excitation, also restricted excitation patterns can be applied, analogous to the reported treatment of C_{60} [14]. The simplest among these patterns, yielding the six $A_g(1)$ peaks, implies the radially symmetrical in-phase displacement of all atoms.

Figure 4 shows the simulated Raman spectrum, obtained by averaging over as many as 20 independent runs,

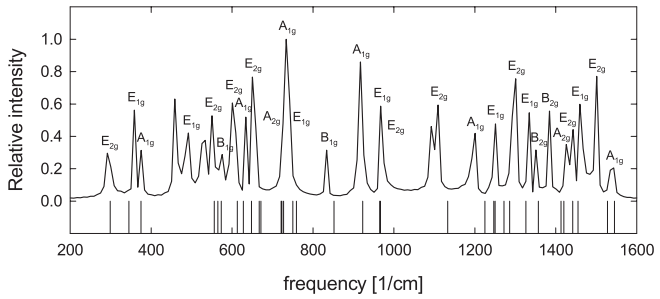

Fig. 4. Calculated power spectrum of C_{36} and Raman frequencies of reference [8].

Table 3. Calculated Raman frequencies of C_{36} (in cm^{-1}) and relative differences $\Delta\nu/\nu^*$ (in %) with respect to those of Jishi *et al.*

Mode	Jishi[a]	Halac[b]		this work	
	ν^*	ν	$\Delta\nu/\nu^*$	ν	$\Delta\nu/\nu^*$
$A_{1g}(1)$	375	332	−11.5	373	−0.5
$A_{1g}(2)$	628	498	−20.7	635	1.1
$A_{1g}(3)$	750	714	−4.8	740	−1.3
$A_{1g}(4)$	923	766	−17.0	909	−1.5
$A_{1g}(5)$	1 225	1 160	−5.3	1 249	2.0
$A_{1g}(6)$	1 545	1 485	−3.9	1 539	−0.4
$E_{1g}(1)$	345	325	−5.8	358	3.8
$E_{1g}(2)$	556	516	−7.2	461	−17.1
$E_{1g}(3)$	721	701	−2.8	652	−9.6
$E_{1g}(4)$	759	814	7.2	730	−3.8
$E_{1g}(5)$	965	873	−9.5	919	−4.8
$E_{1g}(6)$	1 250	1 097	−12.2	1 198	−4.2
$E_{1g}(7)$	1 326	1 307	−1.4	1 333	0.5
$E_{1g}(8)$	1 455	1 454	−0.1	1 461	0.4
$E_{2g}(1)$	299	298	−0.3	295	−1.3
$E_{2g}(2)$	565	551	−2.5	489	−13.5
$E_{2g}(3)$	613	640	4.4	530	−13.5
$E_{2g}(4)$	667	735	10.2	604	−9.4
$E_{2g}(5)$	967	794	−17.9	969	0.2
$E_{2gg}(6)$	1 133	1 034	−8.7	1 107	−2.3
$E_{2g}(7)$	1 286	1 210	−5.9	1 296	0.8
$E_{2g}(8)$	1 442	1 375	−4.6	1 429	−0.9
$E_{2g}(9)$	1 528	1 433	−6.2	1 502	−1.7

[a] Reference [8]. [b] Reference [9].

each started with a random *gerade* initial excitation. No scaling was applied to the resulted frequencies. At the bottom of the panel, the theoretical spectrum of Jishi *et al.* [8], obtained by first-principles calculations, was also depicted by equal-size vertical lines (since no intensity information is available).

The frequencies resulted from the diagonalization of the dynamical matrix agree very well with those yielded by the Fourier analysis of the displacement autocorrelation function. The frequencies of the Raman-active modes have been included in Table 3, along with those of Jishi *et al.* (taken as reference) and those of Halac *et al.* (semi-empirical calculation). For a more eloquent comparison, the relative differences with respect to the frequencies of Jishi *et al.* have been listed, as well. Except

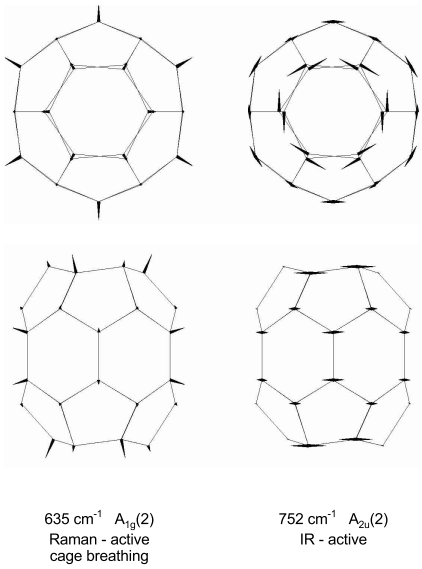

Fig. 5. Atomic displacement patterns for the Raman-active $A_{1g}(2)$ and the IR-active $A_{2u}(2)$ modes of C_{36}.

for the E_{1g} and E_{2g} modes situated in the frequency interval 461–652 cm^{-1}, the relative deviations for all other Raman frequencies obtained in this work do not exceed 5%. The larger discrepancies for the mentioned vibrations are caused by the fact that they involve large-amplitude oscillations of the atoms defining the bonds between the hexagons from the median belt (found slightly elongated as compared to Jishi *et al.*). The deviations corresponding to the results of Halac *et al.* are seen to be typically higher, amounting to over 20% for the "cage breathing" $A_{1g}(2)$ mode.

The superior quality of our results over those of Halac *et al.*, both regarding the geometrical structure and the Raman spectrum, is obviously a direct consequence of the more elaborate TB model on which our calculations are based, but also of the very realistic parametrization of Papaconstantopoulos *et al.* [13] used as part of our approach.

The (scaled) atomic displacements obtained by us for the Raman-active "cage breathing" $A_{1g}(2)$ mode (at 635 cm^{-1}) are displayed in Figure 5, together with those for the IR-active $A_{2u}(2)$ torsion mode (at 752 cm^{-1}).

The IR frequencies yielded by the dynamical matrix are presented in Table 4. Except for the $A_{2u}(4)$, $E_{1u}(1)$ and $E_{1u}(5)$ modes, the relative deviations for all other IR frequencies obtained in this work do not exceed 3.5%. The discrepancies for the mentioned vibrations originate in this case mainly in the large contribution of the oscillations of the atoms defining the long (most distorted) inter-pentagon bonds.

The total number of normal modes we found for the oligomers is 206 for $(C_{36})_2$ and $(C_{36})_3$, and 311 for $(C_{36})_4$. The corresponding Raman spectra, calculated by the Fourier-transform of the displacement autocorrelation function, are shown in Figure 6. For each oligomer the "inter-cage stretch" and the "cage breathing" modes are

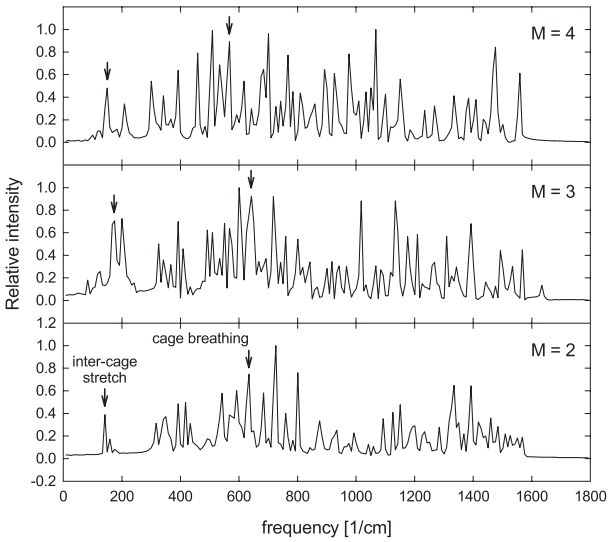

Fig. 6. Calculated Raman spectrum for the most stable oligomers $(C_{36})_{M=2,3,4}$.

Table 4. Calculated IR frequencies of C_{36} (in cm^{-1}).

Mode	Jishi[a]	this work	
	ν^*	ν	$\Delta\nu/\nu^*$
$A_{2u}(1)$	510	511	0.2
$A_{2u}(2)$	758	752	−0.8
$A_{2u}(3)$	785	796	1.4
$A_{2u}(4)$	1 103	1 022	−7.3
$A_{2u}(5)$	1 340	1 385	3.4
$E_{1u}(1)$	459	431	−6.1
$E_{1u}(2)$	483	480	−0.6
$E_{1u}(3)$	668	682	2.1
$E_{1u}(4)$	727	734	1.0
$E_{1u}(5)$	1 083	1 027	−5.2
$E_{1u}(6)$	1 261	1 259	−0.2
$E_{1u}(8)$	1 355	1 375	1.5
$E_{1u}(9)$	1 465	1 454	−0.8

[a] Reference [8].

emphasized. The frequencies and the atomic displacement patterns for these vibrational modes obtained from the dynamical matrix are displayed in Figure 7.

Whereas the patterns for the inter-cage stretch are somehow predictable, in the case of the "cage breathing" the atom oscillations have become rather non-symmetric about the individual cages, departing most for the tetramer from the corresponding monomer pattern. Furthermore, quite opposed to the tetramer, in the dimer and the trimer the atoms forming the inter-cage bonds seem to be practically not involved in the mode, showing very little displacements. In fact, while the dimer and the trimer frequencies remain quite little shifted from the monomer frequency (635 cm^{-1}), the tetramer frequency for this mode is red shifted by as much as 70 cm^{-1}. This is clearly again a consequence of the larger distorsion of the C_{36} cages within the tetramer.

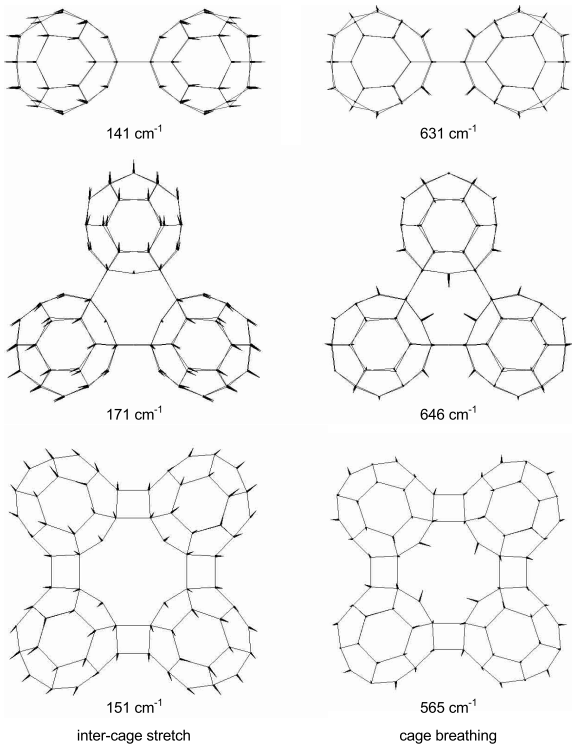

Fig. 7. Atomic displacement patterns for the inter-cage stretch and cage breathing modes of the oligomers $(C_{36})_{M=2,3,4}$.

Along with the experimental spectrum of Piskoti *et al.* [5] obtained for a C_{36} crystalline sample, Figure 8 shows the frequencies calculated in this work for the IR-active modes of C_{36} and its oligomers. Even though our calculations deal with isolated molecular species, in the region between 400 and 900 cm^{-1} the frequencies tend to cluster in four bands, similar to the experimental spectrum. While the monomer can account for the bands around 500, 700, and 800 cm^{-1}, for the band around 600 cm^{-1} seem to be responsible only the oligomers. Furthermore, our calculations suggest major contributions to the band around 1 100 cm^{-1} from the dimer and the tetramer, the monomer being practically not involved.

5 Conclusions

A non-orthogonal TBMD approach is employed to simulate structural and vibrational properties of the C_{36} fullerene molecule and its oligomers $(C_{36})_{M=2,3,4}$. The parametrization used for the Hamiltonian and overlap matrices is the one of Papaconstantopoulos *et al.* [13] and it involves a pseudo-atomic density and environment-dependent on-site and hopping parameters.

The equilibrium structures for all molecular aggregates considered are determined by simulated annealing. The lowest energy isomer of C_{36} is confirmed to have D_{6h} symmetry and the obtained bond lengths agree to within 2.7% (0.04 Å) with the ones resulting from first-principles calculations. All treated oligomers show a well-defined symmetry. For the dimer, the D_{2h} structure reported in the

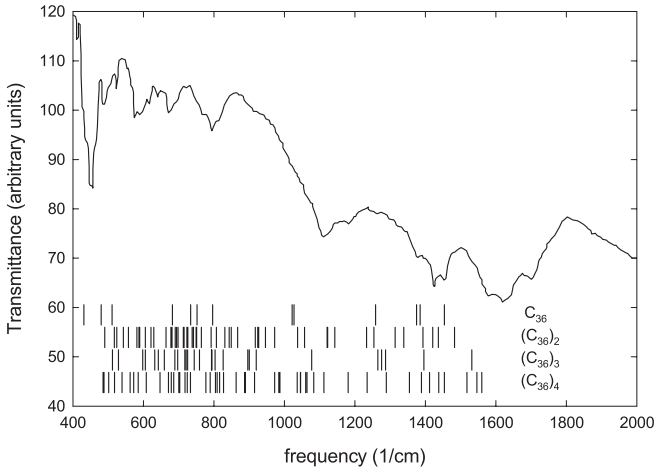

Fig. 8. Experimental IR spectrum for a C_{36} crystalline sample (Ref. [5]) and calculated IR frequencies for C_{36} and its oligomers $(C_{36})_{M=2,3,4}$.

literature is found. Whereas in the dimer and the trimer the individual cages are linked by double bonds, within the tetramer four-fold bonds are formed and the cages are most distorted due to the less adapted symmetry of the environment. The binding energy per atom for the tetramer appears decreased accordingly, rendering it slightly less stable than its predecessors and a less probable building block for larger structures.

To characterize the overall vibration of the molecular structures, the autocorrelation function of the atomic displacements is employed. By initiating the MD runs with random *gerade* excitations, the *gerade* symmetry of the vibration is conserved and the power spectrum of the autocorrelation function is related to the Raman-spectrum. Supplementary information about the vibrational modes is gained by diagonalizing the dynamical matrix. For the monomer fair agreement with reported *ab initio* results is achieved, the relative differences between the vibrational frequencies (not scaled in any way) and the *ab initio* data typically amounting to less than 5%. The atomic displacement patterns for selected normal modes are correlated with the geometric structures and the pseudo-density distribution.

Even though our structural and vibrational results are expected to be slightly less accurate than those from *ab initio* calculations, they are, however, obtained at much lower computational costs and turn out to be superior in most respects to semi-empirical calculations.

References

1. S.C. O'Brien, J.R. Heath, R.F. Curl, R.E. Smalley, J. Chem. Phys. **88**, 220 (1988).
2. G. von Helden, M.T. Hsu, N.G. Potts, P.R. Kemperer, M.T. Bowers, Chem. Phys. Lett. **204**, 15 (1993).
3. K.B. Shelimov, J.M. Hunter, M.F. Jarrold, Int. J. Mass Spectrom. Ion Process. **137**, 17 (1994).
4. L.D. Book, C. Xu, G.E. Scuseria, Chem. Phys. Lett. **22**, 281 (1994).
5. C. Piskoti, J. Yarger, A. Zettl, Nature (London) **393**, 77 (1998).
6. J.C. Grossman, M. Côté, S.G. Louie, M.L. Cohen, Chem. Phys. Lett. **284**, 344 (1998).
7. M. Côté, J.C. Grossman, M.L. Cohen, S.G. Louie, Phys. Rev. Lett. **81**, 697 (1998).
8. R.A. Jishi, M.S. Dresselhaus, Chem. Phys. Lett. **302**, 533 (1999).
9. E. Halac, E. Burgos, H. Bonadeo, Chem. Phys. Lett. **299**, 64 (1999).
10. P.W. Fowler, T. Heine, K.M. Rogers, J.P.B. Sandall, G. Seifert, F. Zerbetto, Chem. Phys. Lett. **300**, 369 (1999).
11. R.E. Cohen, M.J. Mehl, D.A. Papaconstantopoulos, Phys. Rev. B **50**, 14694 (1994).
12. M.J. Mehl, D.A. Papaconstantopoulos, Phys. Rev. B **54**, 4519 (1996).
13. D.A. Papaconstantopoulos, M.J. Mehl, S.C. Erwin, M.R. Pederson, Mat. Res. Soc. Symp. Proc. **491**, 221 (1998).
14. T.A. Beu, J. Onoe, K. Takeuchi, Eur. Phys. J. D **10**, 391 (2000).
15. P. Hohenberg, W. Kohn, Phys. Rev. **136**, B864 (1964).
16. J.C. Slater, G.F. Koster, Phys. Rev. **94**, 1498 (1954).
17. K. Esfarjani, Y. Hashi, J. Onoe, K. Takeuchi, Y. Kawazoe, Phys. Rev. B **57**, 223 (1998).
18. Th. Köhler, Th. Frauenheim, G. Jungnickel, Phys. Rev. B **52**, 11837 (1995).